Structural Controls on Geothermal Reservoir Deformation at Stillwater, Nevada From InSAR and GPS Data

William C. Hammond and John W. Bell

Nevada Bureau of Mines and Geology
University of Nevada, Reno NV

Keywords

Basin and Range, InSAR, GPS, Nevada, Stillwater, geodesy

ABSTRACT

Surface rupture traces of the 1954 Rainbow Mountain earthquake coincide with the western and eastern boundaries of subsidence associated with pumping at the Stillwater, Nevada geothermal plant. Space-based Interferometric Synthetic Aperture Radar (InSAR) provides precise and detailed measurements of surface deformation associated with movement of sub-surface fluids. Maximum peak-to-peak subsidence displacement along satellite radar line of site is near 120 mm for the period March 1, 2009 to August 23, 2009. The oblique-dextral earthquake rupture was consistent in style and orientation with active extension and shear strain accumulation detected with GPS networks in the western Great Basin. The subsidence pattern we detect with InSAR had a compact time-variable subsidence with three distinct lobes, one near the Stillwater, Nevada geothermal plant, another 3 km north of the plant near a well that draws water for the plant, and a third south of the plant that is of unknown origin and of opposite sign. Time series analysis of the interferometric pairs indicates that the most rapid subsidence began before March, 2009. The patterns of subsidence provide evidence that structures related to contemporary tectonic deformation and seismicity play a controlling factor in the location and response to pumping of economically important geothermal resources.

Introduction

The Stillwater area of northern Nevada lies inside the Carson Sink, which is the widest of the tectonically extended basins of the western Basin and Range province. This region is undergoing active tectonic deformation that is measureable with modern geodetic GPS networks (e.g. Hammond et al., 2011; Figure 1). Several productive geothermal facilities are located within the basin, and provide reliable clean power to the electric grid. Located 20 km east of Fallon, NV, the Stillwater geothermal plant,

which went online in 1989, is now owned by Enel Green Power and has a 33 megawatts capacity. Production and pumping at the Stillwater plant continues to this day.

The general location of the Stillwater plant is consistent with a recognized correlation between the active crustal deformation
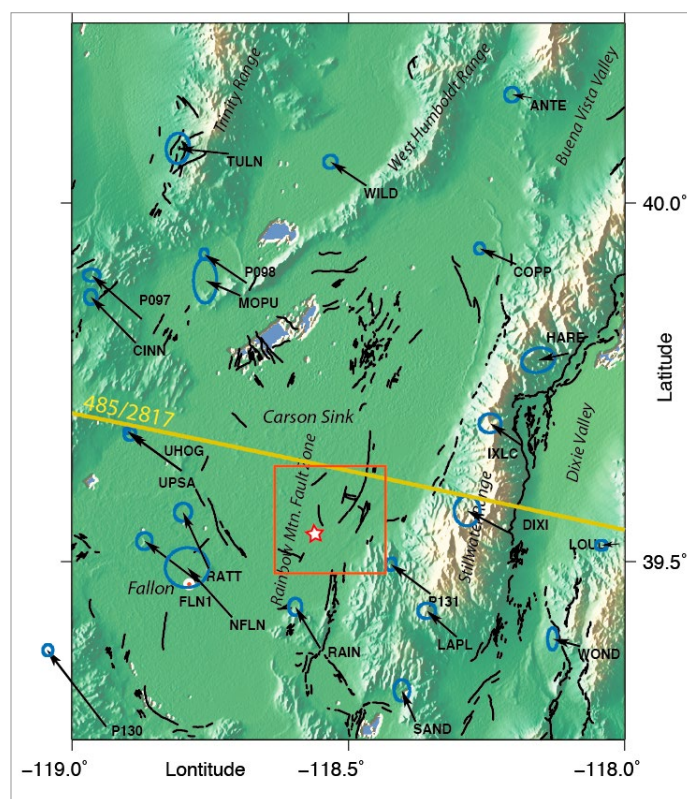

Figure 1. The Stillwater, Nevada geothermal plant (red star) lies within the Rainbow Mountain fault zone. Mapped Mid-Quaternary to historic fault surface ruptures are shown with black lines. Yellow line is the northern boundary of the Envisat track 485, frame 2817 scene used in the InSAR analysis. Black vectors are GPS velocities with respect to the MAGNET network station BIGS which lies in the central Great Basin to the east of the figure, blue ellipses at vector tips are 95% confidence uncertainties in velocity. Orange square indicates boundary of Figure 2 and 3.

field and the presence of geothermal resources (Coolbaugh et al. 2005; Blewitt et al., 2005). We show here that its specific location is also dictated by structural controls associated with the presence of faults in the basin that have slipped in historic time. In particular the Rainbow Mountain (Fallon-Stillwater) earthquake was a part of the sequence of earthquakes that occurred in 1954 that led to recognition of the Central Nevada Seismic Belt as a major cluster of earthquakes in space and time (Bell et al., 2004; Caskey et al., 2004). The 1954 Rainbow Mountain event created surface ruptures that were mapped following the events (Tocher, 1956) and appear to bound a zone of rapid surface deformation related to pumping from wells for geothermal energy production (Figure 2).

A relatively new technology, InSAR measures deformation of the ground surface with a spatial resolution of meters and a deformation-detection precision of millimeters, keeping coherence over months to years (Massonnet, 1994; Bürgmann et al., 2000). Space-based InSAR is very effective at showing the spatial relationship between surface deformation associated with withdrawal of subsurface fluids and other landscape features such as active faults, surficial geology, location of wells, etc. In this study we used InSAR data to measure the time-variable surface deformation between early 2008 and late 2009. We find that over this period a maximum of 120 mm of subsidence occurred. Importantly, the boundary between subsiding and stable portions of the basin are correlated with the mapped traces of surface faults from the Rainbow Mountain earthquake, suggesting structural control from recently active and contemporary tectonic deformation and seismicity on economically important geothermal resources.

Data and Processing

We used 9 radar scenes that were acquired by the European Space Agency ENVISAT mission between May 25, 2008 and August 23, 2009 to form 25 interferograms spanning various overlapping time periods between the first and last scenes. We obtained the data though the WinSAR and GeoEarthScope collections at the UNAVCO SAR archive at http://facility.unavco.org.
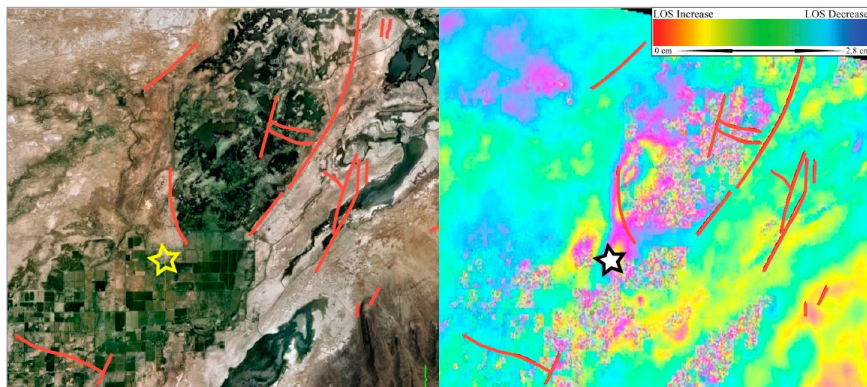
We processed these scenes with the Gamma software package (Werner et al., 2000) by first pre-processing and co-registering the images and then performing two-pass interferometry. We subtracted the topographic radar phase predicted from a 3 arc-second (90 meter) resolution digital elevation model constructed from data of the Shuttle Radar Topography Mission obtained via the U.S. Geological Survey. In an iterative process we refined the solution for satellite orbits to reduce errors in the spacecraft orbital parameters. The interferograms were then unwrapped with a minimum cost function, transformed from radar to geographic coordinates, and converted from radar phase to millimeters of deformation in the satellite line of site, positive toward the satellite. The spacecraft has a look angle of 15°-29° from vertical within the scene so the radar is most sensitive to vertical movement, but also has some sensitivity to horizontal deformation.
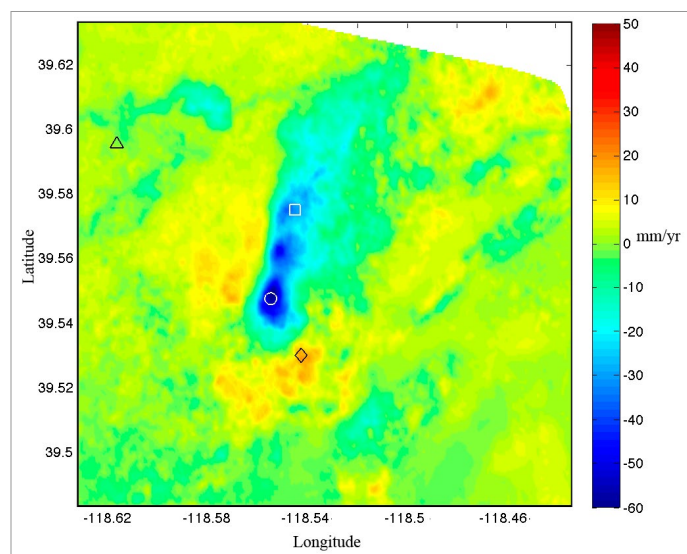

Figure 3. Same region shown in Figure 2 but with a stack of 25 interferograms that shows the average rate of displacement over the interval of time between May 25, 2008 and August 23, 2009. Red is rate towards satellite (up) along line of site, blue away from satellite (down). Circle, square, triangle and diamond show locations where time series analysis results are plotted in Figure 4.

Figure 2. Left) Map showing location of the Stillwater plant (stars) near the southern tip of one of the surface rupture segments of the 1954 Rainbow Mountain earthquake (Tocher, 1956; Caskey et al., 2004). Right) An example wrapped interferogram from Envisat scenes collected on July 19, 2009 and August 23, 2009. The subsidence is indicated by the two-lobed pattern of two blue-red-yellow fringes of coherent line of site increase at and north of the Stillwater plant. A yellow-red-blue fringe (up) lies just to the west of the plant and may reflect re-injection.

We trimmed each scene to include only the area shown in Figures 2 and 3, and performed image conditioning where data gaps were filled, spatial smoothing was applied, and a mean linear phase ramp was removed from each sub-scene. The areas covered by wetland of the Stillwater National Wildlife Refuge generally exhibited poorer interferometric coherence than the dryer adjacent areas of the Carson Sink. We tested the effect of this by applying a mask to remove areas below varying levels of coherence, and found that the images were not sensitive to the level used for the coherence threshold. In the final images we did not remove any values based on coherence. An example interferogram is shown in Figure 2, where the deformation is depicted with color fringes that each represent one half C-band radar wavelength of 5.6 cm, or 2.8 cm.

To obtain the best resolution of the boundaries of the deformation pattern, we formed a stack of all 25 interferograms to estimate the average rate of motion over the entire interval of observation (Figure 3). This essentially double counts some data that are used in multiple interferograms, and does not account for non-linear motion. However, this gross averaging gives the best noise reduction so that deformation patterns may be correlated to geographic features, location of facilities, and patterns in regional faulting.

GPS data in Figure 1 were obtained in 24 hour RINEX format files from several networks including the University of Nevada, Reno Mobile Array of GPS for Nevada Transtension (MAGNET), the NSF EarthScope Plate Boundary Observatory (PBO), the NGS Continuously Operating Reference Network (CORS), and the Washoe County Base Station Control network. The data were processed using the GIPSY OASIS II software made available by the Jet Propulsion Laboratory (JPL), and using JPL's final fiducial-free GPS orbit products (Bertiger et al., 2010). The precise point positioning method was applied to ionospheric-free carrier phase and pseudorange data (Zumberge et al., 1997). Data initially were automatically edited using the TurboEdit algorithm, then at 5-minute intervals carrier phase data were decimated and pseudorange carrier-smoothed (Blewitt, 1990). The time series were aligned to the NA12 North America fixed reference frame (Blewitt et al., 2013) before rates were estimated using the method of Hammond et al., (2011). Rate uncertainties were calculated using the CATS software (Williams, 2003) that includes the contributions from white and flicker noise in the time series model. Finally, we subtracted the horizontal vector rate of GPS station BIGS (which lies at longitude 116.825° west, latitude 39.286° north) to express the velocity with respect to the central Great Basin in order to better portray the variation of rates across the area shown in Figure 1. Processed GPS position time series are now provided free online by the Nevada Geodetic Laboratory for all of these stations, as well as >11,000 other stations globally distributed (_).

Time Series Analysis and Uncertainties

Interferometry measures the difference in ground position between two radar acquisition times along the satellite line of sight look direction. In some cases motion of the ground may be non-linear, i.e. it may change in rate, direction and sign over the period of observation. In these cases simple stacking approaches may yield stable indication of geographic patterns of deformation, but are not designed to infer the time history of the deformation. Furthermore, interferometric pairs are often made from non-adjacent-in-time and overlapping intervals that can make it difficult to infer the true sequence of deformation history.

We reconstructed this history of deformation through time using a linear inversion for the rates of motion between each radar acquisition using the Small Baseline Subset Algorithm (Berardino et al., 2002). Because there are 25 interferograms based on 9 radar scenes that fully connect the time displacement space this inversion is well determined at every location and time interval. The spatial smoothing and gap filling described above ensures that there is an estimate for displacement at each location and each time. After solving for rates of motion we calculate the interval displacements by multiplying by the length of the time intervals between acquisitions. The total cumulative displacement is taken

with respect to an arbitrary starting point (taken to be the position at the first acquisition time August 3, 2008). Thus the first position for each time series is zero (Figure 4).

We perform this analysis on three separate locations. The first is at the generating plant, which is the location of the maximum subsidence of the region covered by Figures 2 and 3 (-118.5553°, 39.5475°). The second point is at the location of a well 3 km north of the main plant (-118.5456°, 39.5750°), and the third was selected as a typical relatively stable location about 6 km west of the main zone of subsidence (-118.6175°, 39.5955°). The result of time series analysis at the third location shows an RMS scatter of reconstructed position of 2.4 mm. Assuming that this location is stable provides an estimate of the uncertainty of the reconstructed line of site position of 2.4 mm. This suggests that the subsidence observed at the other locations is much larger than the uncertainties and is a significant signal in the data.
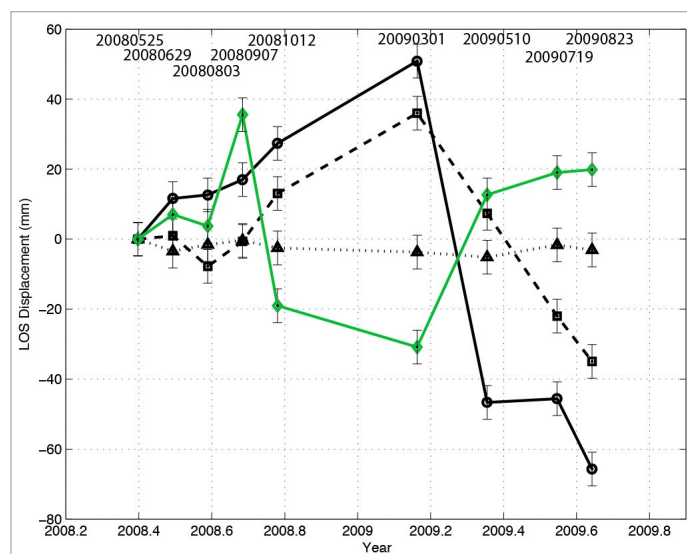

Figure 4. Results of time series analysis showing reconstruction of displacement along satellite line of site as a function of time (positive towards satellite) for four points in the scenes shown in Figures 2 & 3. Time series marked with circles, squares, triangles and diamonds coincide with symbols in Figure 3. Green line with diamonds is for the location showing maximum upward motion in Figure 3. Standard deviation of displacement estimates at a stable location away from Stillwater subsidence (triangles) suggests uncertainty of individual estimates is near 2.4 mm. Maximum subsidence of 120 mm occurs between March 1, 2009 and August 23, 2009. Dates of radar acquisitions are shown at top of figure in *yyyymmdd* format.

Results and Discussion

The areal extent of the subsidence that is observed with InSAR is between 6 and 8 km in length in the north-south direction and 2 to 3 km wide (Figure 3). The subsidence pattern forms two main lobes, one near the Stillwater plant and the other near a well house approximately 3 km north of the plant. Total subsidence at the plant location measured between the maximum position (on March 3, 2009) and minimum (at August 23, 2009) is 120±3 mm (Figure 4). At the second location subsidence occurs over the same time interval but has a smaller total magnitude (72±3 mm).

13

Correlation of the boundary of the subsidence, especially on its western edge, but also on the eastern side, strongly suggest that the geometry of the reservoir is controlled by downward extension of the Rainbow Mountain fault traces in the basin sediments. Collocation of the surface motion with the Stillwater geothermal production wells strongly suggests that the subsidence is attributable to production pumping, however it is possible that there is a component of the deformation that includes a natural seasonal hydrologic cycle. The rise of these points before the March 1, 2009 radar acquisition (Figure 4) may have preceded the initiation of recent Stillwater plant operations, or may reflect re-injection, but detailed comparison with pumping and re-injection timing and volumes will require analysis of records we have not yet obtained.

We observe upward signals just west of the Stillwater plant and at another location southeast of the plant (-118.543°, 39.530°). These are shown as areas with mean upward trends (red in Figure 3). However, with the exception of the measurement on September 2008, the motion is down then up, taking the opposite sign of the larger net subsidence feature to the north near the production well. Thus these two areas are subsiding when the ground to the north is rising, and vice-versa (green line Figure 4). They are not near wells known by us to be associated with the Stillwater geothermal production, but are likely related to rising water levels or from recovery of depressed water levels from pumping or from recharge. Given the temporal resolution of InSAR, the evolution of the subsidence may have been more complicated than illustrated in Figure 4, but the trends are usually consistent in direction of motion over periods of ~6 months before and after March 1, 2009.

The Rainbow Mountain fault zone is a long, widely distributed fault zone that has numerous sub-parallel, oblique to left-stepping intra-basin faults that occur throughout much of the Carson Sink and along the margin of the Salt Wells Basin to the south. These faults ruptured during the three-event 1954 Rainbow Mountain-Fourmile Flat-Stillwater sequence (Tocher, 1956; Caskey et al., 2004), having magnitudes estimated to be MS 6.3, M 6.4 and MS 7.0 respectively. The 1954 rupture pattern and two prehistoric events discovered in trenches at Rainbow Mountain suggest that these faults form a discrete fault zone that may be related to the Eastern Carson Sink fault zone and to unnamed faults in Salt Wells Basin. Right-oblique surface faulting associated with the three events together formed a 70-km-long, left-stepping pattern from Rainbow Mountain north into the Carson Sink and southeast into Fourmile Flat (Bell et al., 2004).

The deformation patterns we have imaged using InSAR may suggest that the Rainbow Mountain faults are deep structures that connect at depth and together contribute to accommodating a significant amount of the deformation budget of the Northern Walker Lane and western Basin and Range. Thus these results bear on the question of whether most strain associated with Basin and Range tectonic deformation is released in earthquakes on major range-bounding faults or whether a significant proportion of the strain is released on faults that cut basin floors. This question has recently come under renewed debate and scrutiny as more careful comparisons are made between geodetic and geologic measures of deformation (Wesnousky et al, 2012). If the discontinuous rupture traces of the active Rainbow Mountain fault system extend and

connect at depth, then this fault system that continues northward through the Carson Sink, and southward through the Fourmile Flat area, may represent an important and long-lived system system. The implications for prospecting for geothermal energy in the Great Basin are considerable since these systems host economically important geothermal resources.

Acknowledgements

References

Bell, J. W., S. J. Caskey, A. R. Ramelli, and L. Guerrieri (2004), Pattern and rates of faulting in the central Nevada seismic belt, and paleoseismic evidence for prior belt-like behavior, *Bulletin of the Seismological Society of America*, *94*, 4, 1229-1254.

Berardino, P., G. Fornaro, R. Lanari, and E. Sansosti (2002), A new algorithm for surface deformation monitoring based on small baseline differential SAR Interferograms, *IEEE Transactions on Geoscience and Remote Sensing*, *40*, 11, 2375-2383.

Bertiger, W., Desai, S.D., Haines, B., Harvey, N., Moore, A.W., Owen, S., and Weiss, J.P. (2010), Single receiver phase ambiguity resolution with GPS data, *J. Geodesy,* 84(5), 327-337, doi: 101007/s00190-010-0371-9.

Blewitt, G. (1990), An automatic editing algorithm for GPS data, *Geophysical Research Letters*, *17(3)*.

Blewitt, G., W. C. Hammond, and C. Kreemer (2005), Relating geothermal resources to Great Basin tectonics Using GPS, *Geothermal Resource Council Transactions*, *29*, 331-335.

Blewitt G., H.-P. Plag, Y. Bar-Sever, C. Kreemer, W.C. Hammond, J. Goldfarb, GPS time series in ITRF and derivative frames: Trade-offs between precision, frequency, and latency, EGU General Assembly, Vienna, Austria, April 7-12, *Geophysical Research Abstracts, v*. 15, 2013.

Bormann, J., W.C. Hammond, G. Blewitt, C. Kreemer, S. Jha, A synoptic model of fault slip rates in the Eastern California Shear Zone and Walker Lane from GPS velocities for seismic hazard studies, SSA Annual Meeting, Salt Lake City, Utah, April 17-19, 2013.

Bürgmann, R., P. Rosen, and E. J. Fielding (2000), Synthetic Aperture radar interferometry to measure Earth's surface topography and its deformation, *Annual Review of Earth and Planetary Science*, *28*, 169-209.

Caskey, S. J., J. W. Bell, S. G. Wesnousky, and A. R. Ramelli (2004), Historic surface faulting and paleoseismicity in the area of the 1954 Rainbow Mountain–Stillwater earthquake sequence, central Nevada, *Bulletin of the Seismological Society of America*, **94,** no. 4, 1255–1275.

Coolbaugh, M., R. Zehner, C. Kreemer, D. D. Blackwell, G. Oppliger, D. Sawatzky, G. Blewitt, A. Pancha, M. Richards, C. Helm-Clark, L. Shevenell, G. Raines, G. Johnson, T. Minor, and T. Boyd (2005), Geothermal potential map of the Great Basin region, western United States.

Hammond, W. C., G. Blewitt, and C. Kreemer (2011), Block modeling of crustal deformation of the northern Walker Lane and Basin and Range from GPS velocities, *Journal of Geophysical Research, 116, B04402, doi:10.1029/2010JB007817.*

Kent, Tyler, Comparing Deformation at Soda Lake Geothermal Field from GPS and 3D Seismic, Master Thesis, University of Nevada, Reno, unpublished.

Massonnet, D., K. Feigl, M. Rossi, and F. Adragna (1994), Radar Interferometric Mapping of Deformation in the Year after the Landers Earthquake, *Nature*, *369*, 6477, 227-230.

Tocher, D. (1956), Movement on the Rainbow Mountain fault, *Bull. Seism. Soc. Am.* **46,** 10–14.

Werner, C., U. Wegmuller, T. Strozzi, and A. Wiesmann (2000), Gamma SAR and interferometric processing software, *ERS-ENVISAT Symposium, European Space Agency, Gothenberg, Sweden*.

Wesnousky, S. G., J. Bormann, C. Kreemer, W. C. Hammond, and J. N. Brune (2012), Neotectonics, geodesy, and seismic hazard in the Northern Walker Lane of Western North America: Thirty kilometers of crustal shear and no strike-slip?, *Earth and Planetary Science Letters*, *doi:10.1016/j.epsl.2012.02.018*.

Williams, S. P. D. (2003), The effect of coloured noise on the uncertainties of rates estimated from geodetic time series, *Journal of Geodesy*, *76*, 483-494.

Zumberge, J. F., M. B. Heflin, D. C. Jefferson, M. M. Watkins, and F. H. Webb (1997), Precise point positioning for the efficient and robust analysis of GPS data from large networks, *Journal of Geophysical Research*, *102*, B3, 5005-5017.